hydrogen

MDPI

Article

Impact of the Anode Serpentine Channel Depth on the Performance of a Methanol Electrolysis Cell

Vladimir L. Meca [1,2,*], Elena Posada [2], Antonio Villalba-Herreros [1,2], Rafael d'Amore-Domenech [1,2], Teresa J. Leo [1,2] and Óscar Santiago [3]

[1] Department Arquitectura, Construcción y Sistemas Oceánicos y Navales, ETSI Navales, Universidad Politécnica de Madrid, Avenida de La Memoria 4, 28040 Madrid, Spain; antonio.villalba@upm.es (A.V.-H.); r.damore@upm.es (R.d.-D.); teresa.leo.mena@upm.es (T.J.L.)

[2] Grupo de Investigación UPM Pilas de Combustible, Tecnología Del Hidrógeno y Motores Alternativos (PICOHIMA), ETSI Navales, Universidad Politécnica de Madrid, Avenida de La Memoria 4, 28040 Madrid, Spain

[3] Research Group Environmental Process Engineering, Center for Environmental Research and Sustainable Technology (UFT), University of Bremen, Leobener Str. 6, 28359 Bremen, Germany; santiago@uni-bremen.de

* Correspondence: vl.meca@upm.es

Abstract

This work addresses for the first time the effect of anode serpentine channel depth on Methanol Electrolysis Cells (MECs) and Direct Methanol Fuel Cells (DMFCs) for improving performance of both devices. Anode plates with serpentine flow fields of 0.5 mm, 1.0 mm and 1.5 mm depths are designed and tested in single-cells to compare their behaviour. Performance was evaluated through methanol crossover, polarization and power density curves. Results suggest shallower channels enhance mass transfer efficiency reducing MEC energy consumption for hydrogen production at 40 mA·cm^{-2} by 4.2%, but increasing methanol crossover by 30.3%. The findings of this study indicate 1.0 mm is the best depth among those studied for a MEC with 16 cm^2 of active area, while 0.5 mm is the best for a DMFC with the same area with an increase in peak power density of 14.2%. The difference in results for both devices is attributed to higher CO_2 production in the MEC due to its higher current density operation. This increased CO_2 production alters anode two-phase flow, partially hindering the methanol oxidation reaction with shallower channels. These findings underscore the critical role of channel depth in the efficiency of both MEC and DMFC single-cells.

Keywords: Hydrogen production; methanol; fuel cell; electrolyser; anode flow field design; single serpentine flow field

Academic Editors: Bahman Shabani and Mahesh Suryawanshi

Received: 26 June 2025
Revised: 12 July 2025
Accepted: 17 July 2025
Published: 19 July 2025

Citation: Meca, V.L.; Posada, E.; Villalba-Herreros, A.; d'Amore-Domenech, R.; Leo, T.J.; Santiago, Ó. Impact of the Anode Serpentine Channel Depth on the Performance of a Methanol Electrolysis Cell. *Hydrogen* **2025**, *6*, 51. https://doi.org/10.3390/hydrogen6030051

1. Introduction

The increasing concern over the energy crisis and climate change has sparked a heightened societal interest in exploring alternative fuels and energy sources to diminish pollutant emissions and reduce reliance on fossil fuels [1]. Renewable energy sources are gaining prominence in national and international energy strategies due to their low environmental impact. However, technologies such as solar and wind are inherently intermittent and geographically constrained, often generating electricity far from end users and at times misaligned with demand. To address these temporal and spatial mismatches, it is necessary to implement energy conversion and storage systems capable of integrating renewables into existing power grids [2]. One effective strategy is to convert excess renewable electricity

into chemical energy in the form of hydrogen through water electrolysis. Hydrogen thus serves as a flexible energy carrier, enabling both the storage of surplus energy and its transport over long distances, while also providing a clean fuel for downstream applications such as fuel cells. Thus, the global push towards sustainable energy solutions has accelerated research into low-carbon energy carriers and efficient storage methods [3]. In this context, hydrogen is valued for its clean use in fuel cells, producing only water as a byproduct during its operation [4,5]. However, the practical challenges associated with hydrogen, such as its low volumetric energy density and the need for storage under high pressures or cryogenic temperatures, highlight the need for complementary solutions to facilitate its adoption on a large scale. Methanol, among these alternatives, stands out as one of the most attractive [6], offering an appealing alternative and complement to hydrogen in the landscape of energy carriers [7], particularly due to its favorable physical properties [8]. As a liquid at ambient temperature and pressure, methanol is easier and safer to transport, which facilitate its handling, distribution, storage and refueling [9,10]. Its physical characteristics combined with its energy density, 17.8 $GJ \cdot m^{-3}$, and specific energy, 22.7 $MJ \cdot kg^{-1}$, position methanol as an appropriate candidate for long-term energy storage, potentially leveraging existing petroleum infrastructure for distribution [10,11]. The concept of a methanol-based renewable-powered energy chain aims to convert surplus renewable electricity into a versatile, transportable and storable energy form: methanol. This process starts with the use of renewable energy sources, such as solar or wind, to produce hydrogen through electrolysis, splitting water molecules into hydrogen and oxygen. The hydrogen generated through this clean process can then be combined with carbon dioxide (CO_2) captured directly from the atmosphere. By combining hydrogen and captured CO_2, e-methanol can be synthesized, obtaining a renewable liquid fuel [10,12–14]. The methanol produced in this way serves as a highly useful energy carrier. E-methanol offers a pathway to store renewable energy in a stable, dense form that is easy to handle and ship over long distances. During transport or once in the destination where it is needed, methanol can be utilized both directly as a fuel, as in Direct Methanol Fuel Cells (DMFCs), and indirectly as a hydrogen carrier through methanol cracking, methanol reforming or methanol electrolysis processes [15–18]. These properties positions methanol as an effective medium for energy storage, particularly where decentralized or off-grid hydrogen production is desired. In fact, the use of methanol electrolysis enables on-demand hydrogen production at lower temperatures and pressures than methanol reforming processes, making it feasible to generate hydrogen closer to the point of use with methanol electrolyzers. This renewable hydrogen can then be used as a clean fuel for various applications, including fuel cells or industrial processes, providing an effective, closed-loop cycle for renewable energy use and storage. This power-to-methanol link enables a sustainable, circular approach to energy: renewable electricity is stored in the form of methanol, which can be transported and later converted back into hydrogen. This system not only leverages the strengths of renewable sources but also enhances the practical storage, transport and deployment of clean energy in a flexible and scalable manner.

In terms of storage, methanol does not require heavy, bulky pressurized tanks. Instead, the containers can adopt various shapes, adapting to the available spaces within systems, allowing for more compact and versatile designs [19–21]. Furthermore, worldwide methanol production has been on a continuous annual growing during recent years, exceeding 100 million tons, and its market potential for 2026 has been estimated at $91.5 billion globally, demonstrating the great interest it has aroused and its availability around the world [10].

As previously mentioned, methanol can be utilized not only as a hydrogen carrier but also as a direct fuel. One alternative for its use at the destination, instead of hydrogen pro-

duction, is to produce electricity directly from methanol [22]. This can be achieved through technologies such as DMFCs, which enable the electrochemical conversion of methanol into electricity without intermediate steps. In this configuration, methanol functions as an energy carrier, offering a compact and efficient solution for decentralized power generation and portable applications [23]. This approach is particularly advantageous in off-grid or remote applications, where operational simplicity, flexibility and minimized infrastructure are critical.

The operation of DMFCs involves a methanol oxidation reaction at the anode, see Equation (1), producing CO_2 as the primary product while releasing electrons that flow through an external circuit and protons that cross the membrane to the cathode. At the cathode, an oxygen reduction reaction occurs, see Equation (2), involving the electrons and protons generated at the anode to produce water [1,24–26]. The combination of these reactions, see Equation (3), is thermodynamically spontaneous.

$$\text{Anode}: \ CH_3OH + H_2O \rightarrow CO_2 + 6H^+ + 6e^- \quad (1)$$

$$\text{Cathode}: \ \frac{3}{2}O_2 + 6e^- + 6H^+ \rightarrow 3H_2O \quad (2)$$

$$\text{Overall}: \ CH_3OH + \frac{3}{2}O_2 \rightarrow CO_2 + 2H_2O \quad (3)$$

DMFCs have been extensively studied over the last two decades, leading to the development of modules with power ranging from tens of milliwatts to 2500 W [27–32]. As power sources, their primary use is geared towards low-power portable applications, such as smartphones, laptops, unmanned aerial vehicles or autonomous underwater vehicles [33].

Despite the interest generated by DMFCs, there are still technical issues limiting their widespread commercialization. Among these limitations are the high cost of catalysts and membranes, slow reaction kinetics, methanol crossover through the membranes, or degradation, which is a complex issue that impacts their performance and lifespan, even maintenance and replacement costs [34–36]. To address these limitations, various strategies are being pursued, such as the development of new non-platinum group catalysts or the synthesis of hybrid membranes [26]. However, aside from these strategies, another approach to enhance DMFC performance involves optimizing the fluid fields of bipolar plates to improve mass transport to and from the electrodes [37–40]. Thus, the flow field of the plates has an influence on the distribution of the fuel and the oxidant, and the elimination of the water and CO_2 formed during the reactions [35,41,42]. A wide range of geometries has been studied to enhance reactant distribution onto the catalytic layer, being the most investigated parallel, serpentine, interdigital and bio-inspired configurations [37,43–45]. Among them, serpentine flow-field is the most used in DMFCs due to its efficiency in removing reaction products, enhancing two-phase mass transport, preventing gas blockages and improving flow under the ribs [35,46,47]. On the contrary, it suffers from high pressure drop and may exhibit a significant concentration gradient between the inlet and outlet [35,47–49].

One of the parameters of the serpentine flow field with the greatest influence on DMFC performance is the channel depth. Yu et al. [50] demonstrated that, for the same flow rate, reducing the channel depth to at least 0.5 mm results in an improvement in electrochemical performance, especially at high current densities. This effect can be explained based on the improvement of the mass transfer. However, with a given flow rate, the rise in methanol velocity due to the reduction in depth and, consequently, in pressure, results in increased methanol crossover through the membrane, leading to a decline in performance, particularly at low current densities as lower amount of methanol is consumed [43,51,52]. Additionally, the presence of two-phase flow, liquid methanol-water mixture and gaseous

CO_2, in the anode field make difficult the distribution of reactants to the catalytic surface and the removal of the products [34,41–43]. The presence of the produced CO_2 can cause a gas accumulation, even a blockage, which impedes methanol and water from efficiently reaching the catalyst surface where the electrochemical reaction takes place. This can cause a non-uniform distribution of the reactants and, therefore, a lower efficiency in energy generation. Moreover, if this CO_2 layer is not properly removed, it can clog the active sites of the catalyst and reduce the efficiency of the reaction. If the dimensions of the anode side channels in a DMFC are reduced, these channels can easily become filled with CO_2 bubbles, forming slugs. These bubbles can hinder the methanol mass transport to the anode catalyst layer, especially at low flow velocities, which in turn can lead to high overpotentials at high current densities [51,52]. Thus, the two-phase flow regime depends on the velocity [43,53,54].

Nevertheless, DMFCs have a limited range of application due to their low power output. When higher power is required, alternatives such as hydrogen fuel cells can be considered. In this context, a methanol electrolysis cell (MEC) can be used to produce hydrogen, capitalizing on the fact that less energy is needed to produce hydrogen through methanol electrolysis compared to water electrolysis [55–57]. This outlines a scenario where methanol, with its high energy density and ease of handling, distribution and storage, can be used as an energy carrier. This allows for the transportation of energy to subsequently produce hydrogen on-site at a lower energy cost [58–60].

While the oxidation reaction in the MEC is the same as in the DMFC, see Equations (1) and (4), the main difference lies in the reduction reaction. In this case, unlike in the DMFC, the reduction reaction leads to the production of molecular hydrogen, as shown in Equation (5) [56,61]. Similar to water electrolysis, methanol electrolysis is a non-spontaneous process requiring an input of energy, with the minimum potential difference under standard conditions at 25 °C being 0.02 V [62,63].

$$\text{Anode}: \ CH_3OH + H_2O \rightarrow CO_2 + 6\,H^+ + 6\,e^- \tag{4}$$

$$\text{Cathode}: \ 6\,e^- + 6\,H^+ \rightarrow 3\,H_2 \tag{5}$$

$$\text{Overall}: \ CH_3OH + H_2O \rightarrow CO_2 + 3\,H_2 \tag{6}$$

Unlike DMFCs, MECs are devices that have hardly been explored so far, with most research focusing on the optimization of operating parameters and the development of catalysts for hydrogen reduction reaction rather than flow field optimization [63–65]. However, transport phenomena and CO_2 bubble regimes could change drastically, and consequently the optimal flow field configuration, due to the significant difference in current densities achieved in MECs (around 400 $mA{\cdot}cm^{-2}$ or even higher) compared to DMFCs (up to 200 $mA{\cdot}cm^{-2}$) and therefore in CO_2 generation. Thus, the study of those configurations in MECs is of great scientific and technical interest to improve MEC efficiency.

The aim of this work is to compare the influence of the anode channel depth of a serpentine flow field on the electrochemical performance of a DMFC and, for the first time, on the performance of a MEC, as well as on methanol crossover through the membrane. For this purpose, single serpentine channels are machined in stainless steel 316L plates designed specifically for the methanol electrochemical devices. In the case of the cathodic plate, the channel depth used is 0.5 mm, but in the case of anodic plates, three different depths are studied: 0.5 mm, 1.0 mm and 1.5 mm. A series of experiments was designed to obtain the polarization curves for DMFC and MEC configurations and measure the limiting methanol crossover current density.

2. Materials and Methods

Figure 1 shows an exploded view of the electrochemical cell used in this study as DMFC, MEC and for the measurement of the limiting crossover current density. The electrochemical cell consists of two stainless steel 316L plates, two silicone gaskets (thickness: 0.2 mm in the anode side, 0.1 mm in the cathode side) and a membrane electrode assembly (MEA) with an active area of 16 cm^2. The MEAs used are formed by Nafion 117 as proton exchange membrane (H2planet, Vizcaya, Spain), sandwiched between an anode (3.0 $mg \cdot cm^{-2}$ Pt/Ru, molar ratio 1:1) and a cathode (1.0 $mg \cdot cm^{-2}$ Pt). For the DMFC and limiting crossover current density experiments, the electrodes are supplied by Quintech (anode: BC-H225-10F and cathode: BC-M100-30F). For the MEC experiments the electrodes are prepared following the protocol described by Jurado et al. [66] using Toray H60 (Alfa Aesar, Haverhill, MA, USA) as substrate and with catalysts from Pi-Kem (Tamworth, UK). The MEAs are prepared using the hot-pressing technique, applying a pressure of 60 bar with a MEGA MGH-30 hydraulic jack, while maintaining the plates at 130 °C for 3 min.

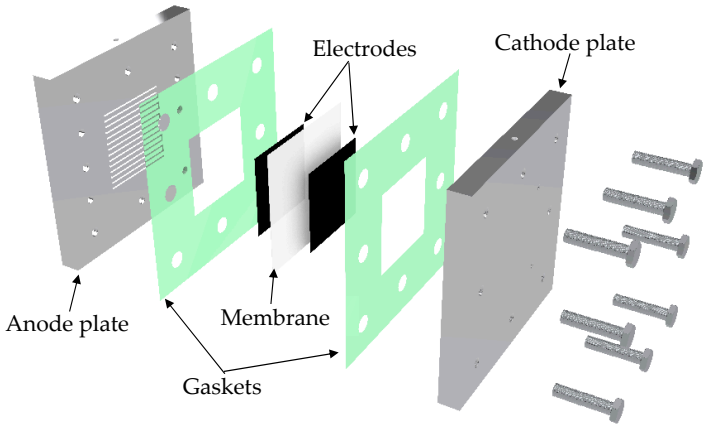

Figure 1. Exploded view of the designed and fabricated in-house single-cell studied in this work.

Figure 2 shows a CAD drawing of the front view of the 100 × 100 × 10 mm^3 stainless steel plate used as current collector with detailed sections of the serpentine flow field. It features a single serpentine flow field with 24 turns of 180° machined in the central zone, covering a 40 × 40 mm^2 area with an open ratio and channel and rib thicknesses of 62.4%, 1.0 mm and 0.6 mm, respectively. All the plates used have an N3 surface treatment in the contact area. In both, DMFC and MEC experiments, the serpentine of the cathode side always has a depth of 0.5 mm. Conversely, three plates for the anode side have been tested with three different depths to analyze their influence on the performances of both types of cells (see detail D in Figure 2). Table 1 summarizes the single-cell configurations and the dimensions of the channels used in this study. The assembly is clamped by means of eight M5 screws, applying 1.5 N·m torque. Additionally, the cells have three nylon bolts for the proper positioning of the plates.

Table 1. Specifications of the cell configurations studied in this work.

Parameter	Plate 1	Plate 2	Plate 3
Depth of anode channel, mm	0.5	1.0	1.5
Depth of cathode channel, mm	0.5	0.5	0.5
Material of the plates	SS316L	SS316L	SS316L
Number of channel bends	24	24	24
Width of anode channel, mm	1.0	1.0	1.0
Open Ratio of anode channel	0.624	0.624	0.624
Contact surface treatment	N3	N3	N3

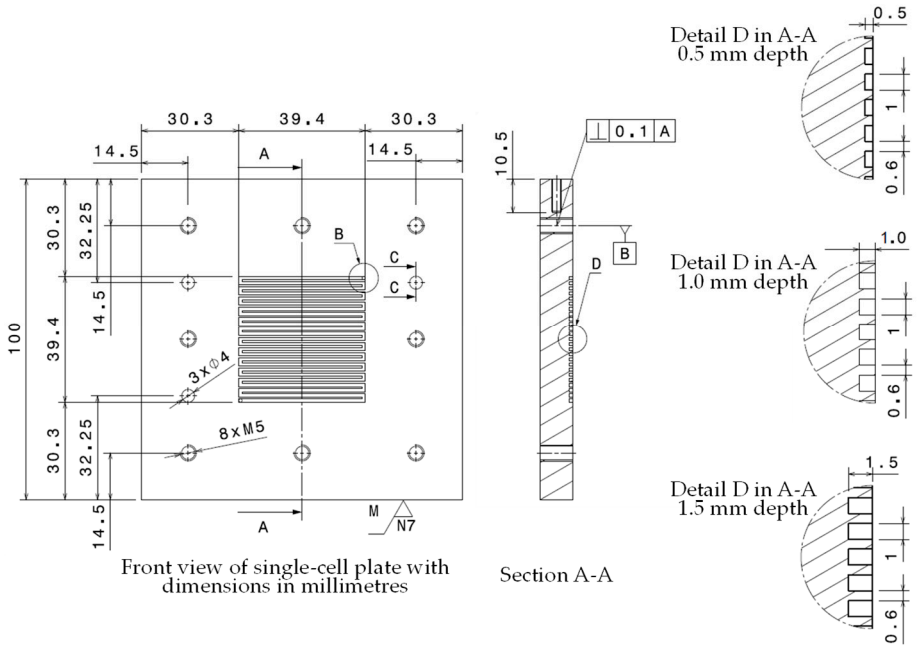

Figure 2. CAD drawing of single-cell anode plate with key dimensions and details of serpentine flow field sections for the three channel depth values under study.

To assess the electrochemical performance of DMFCs and MECs, polarization curves had been recorded. These measurements had been conducted at 60 °C for both, DMFC and MEC, supplying 1 M methanol solution at 3 mL·min^{-1} to the anode and, in the case of DMFC, pure oxygen humidified at 68 °C at 110 mL·min^{-1} and 0.1 MPa to the cathode. In the case of MEC, no solution or gas had been supplied to the cathodic side of the device. Excess reactants had been provided to prevent potential mass transfer losses. The methanol (99.9% purity) was supplied by PanReac AppliChem (Castellar del Vallès, Barcelona, Spain) while the oxygen (purity higher than 99.5%) was provided by Messer Iberica de Gases (Vila-seca, Tarragona, Spain). Milli-Q grade water was used to prepare the methanol-water solutions. Flow directions within the cell significantly impact reactant distribution and temperature due to reactant consumption and the presence of two-phase flow on both sides [38]. Thus, the methanol solution had been supplied to the anode from bottom to top, against gravity, facilitating CO_2 removal by means of the natural pressure gradient [50]. Analogously, the oxygen had been supplied to the DMFC cathode from top to bottom to aid in evacuating the liquid water produced, preventing cathode channels flooding [38]. Table 2 summarizes the general operational parameters and the components utilized in the MEAs of DMFC and MEC to assess the influence of anode channel depths on electrochemical performance.

The DMFC polarization curve measurements had involved monitoring the current of a single-cell while adjusting the applied voltage in decreasing steps of 20 mV, starting at 660 mV and lasting for 180 s per step. These measurements were conducted using a custom-built test bench, as previously described in literature [67]. In contrast, MEC polarization curves were recorded using a custom-built test bench [68] based on the use of an Autolab PGSTAT128N potentiostat-galvanostat connected to a Booster10A module under galvanostatic operation, ranging from 0 mA·cm^{-2} to 400 mA·cm^{-2} with steps of 20 mA·cm^{-2}, with each current being applied over 180 s. PGSTAT128N presents a voltage and current measurement accuracy of ± 0.2%. For each of the three DMFC configuration, a total of 31 polarization curves had been obtained plus 2 activation curves, ranging from open circuit potential to 0.4 V, conducted on the initial day of operation of each configuration. Conversely, in the MEC single-cell experiments, 8 curves had been recorded

for each configuration, due to the comparatively lower variation observed among the results between curves.

Table 2. Parameters used during the experimental tests developed in this work in Direct Methanol Fuel Cells (DMFCs) and Methanol Electrolysis Cells (MECs).

Parameter	DMFC	MEC
Temperature, °C	60	60
Methanol concentration, mol·L^{-1}	1	1
Methanol flow rate, mL·min^{-1}	3	3
Methanol supplier	Panreac AppliedChem (99.9%)	Panreac AppliedChem (99.9%)
Oxygen flow rate, mL·min^{-1}	110	-
Oxygen pressure, MPa	0.1	-
Anode catalyst	Pt/Ru, molar ratio 1:1	Pt/Ru, molar ratio 1:1
Anode catalyst charge, mg·cm^{-2}	3	3
Anode commercial reference	BC-H225-10F	-
Anode supplier	Quintech	-
Cathode catalyst	Pt	Pt
Cathode catalyst charge, mg·cm^{-2}	1	1
Cathode commercial reference	BC-M100-30F	-
Cathode supplier	Quintech	-

The determination of the limiting crossover current density had followed the method previously outlined by Ren et al. [69] and used to compare several membranes behaviour against methanol crossover [70]. The methanol aqueous solution 1 M had been supplied to the anode side of the fuel cell at 3 mL·min^{-1}, while pure nitrogen, humidified at 68 °C, had been supplied to the cathode side of the fuel cell at a flow rate of 110 mL·min^{-1}. An Autolab PGSTAT128N potentiostat-galvanostat had been operated in potentiostatic mode to record the current response to the applied potential, ranging from 0.3 V to 0.95 V in steps of 50 mV applied over 180 s. In this setup, the electrode typically serving as the DMFC cathode has acted as the working electrode, polarising to catalyse the oxidation reaction of the methanol crossing the membrane. Meanwhile, on the opposing electrode, which serves as the counter electrode and the reference electrode, a hydrogen evolution process had occurred. Consequently, the detected electrical current had resulted from the oxidation of methanol that had crossed the membrane.

3. Results

In this section, the outcomes of the polarization and power density curves obtained from the DMFC and MEC single-cell experiments are presented, as well as the comparisons of power densities, slopes and open circuit potentials for the different anode channel depths. The methanol crossover is also assessed for each of the channel depths by means of the limiting crossover current density comparison. The DMFC polarization curves presented here, along with their derived data, are obtained by calculating the average and the 95% confidence interval of the three polarization curves that achieve the highest power density on different days. The data for the MEC polarization curves is obtained by averaging and taking the 95% confidence interval of the last three curves obtained for each channel depth.

3.1. Crossover

Crossover denotes the passage of methanol from the anode side of the MEA to the cathode without reacting, thereby diminishing the fuel efficiency of the cell due to the loss of part of the methanol that is not oxidized at the anode and that, on reaching the cathode, reacts with oxygen reducing the cathode potential [71,72]. Figure 3 shows the current

density resulting from methanol oxidation crossing the membrane against the applied potential. The maximum current density observed for each depth represents its respective limiting crossover current density. According to Figure 3, a reduction in channel depth is linked to a significant increase in crossover. Thus, a reduction in the depth from 1.5 mm to 0.5 mm results in a 30.3% rise in the limiting crossover current density. This notable increase in crossover could be associated with the heightened dynamic pressure in the channel [73], theoretically nine times higher for a 0.5 mm depth channel compared to a 1.5 mm channel. This favors the convective transport of methanol through the membrane as the pressure on the cathodic side remains constant for all configurations.

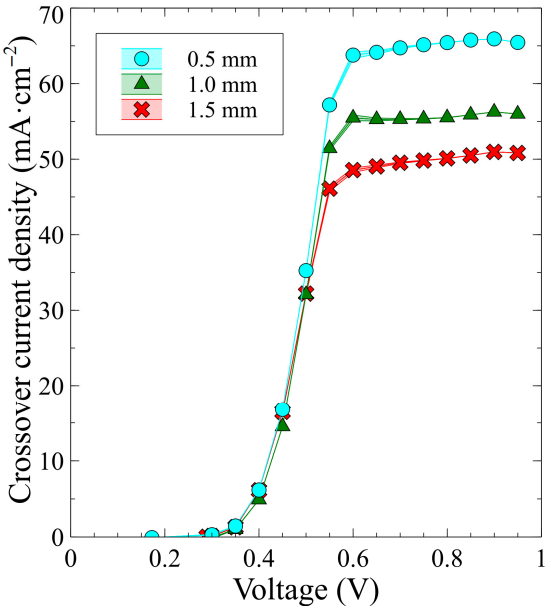

Figure 3. Crossover current density with 0.5 mm, 1.0 mm and 1.5 mm of anode channel depth, results obtained at a temperature of 60 °C, cathode pressure 0.1 MPa, nitrogen flow rate of 110 mL·min^{-1}, a methanol concentration of 1 M and methanol flow rate of 3 mL·min^{-1}.

Additionally, a shorter diffusion distance, with shallower channels, means that the path that methanol must take to diffuse from one side of the MEA to the other is shorter. This facilitates diffusion across the membrane or electrode, which can increase the chance of crossover occurring. It is worth mentioning that the experimental technique used to determine the limiting crossover current density is only used to study the crossover produced in DMFC and MEC at low current densities. This is because operating at high current densities results in significant methanol consumption at the anode which is not replicated in this experiment.

The methanol crossover can substantially impact the performance of both DMFCs and MECs, particularly at low power densities. It diminishes methanol utilization at the anode in both cases while potentially affecting the electrochemical yield of the cathode. Regarding this, high crossover in a DMFC might lead to a reduction in fuel cell potential, whereas in the case of a MEC, it could influence its performance as well as the purity of the obtained hydrogen.

3.2. Methanol Electrolysis Cell

The polarization curves elucidate the voltage-current relationship during the operation of the devices across various depths of anode channels. Power density curves, derived from these polarization curves, quantify the electric energy consumed (MEC) or generated (DMFC) per unit of active area.

Comparing the MEC polarization curves presented in Figure 4 for different channel depths, it is possible to conclude that for current densities below 80 mA·cm^{-2} the curve with the lowest voltage for a given current density corresponds to a 0.5 mm channel depth. This is in good agreement with the results previously reported by Lamy et al. [74] for MECs using, as in this study, Nafion 117 as membrane. In their work, the potential required for the electrolysis process at low current densities decreases as the concentration of methanol in the anode increases from 0.5 M to 10 M, and consequently, the crossover increases too. In fact, comparing the results reported in Figure 4 for anode channel depths of 1.5 mm and 0.5 mm, at 80 mA·cm^{-2} there is a reduction of 2.5% in the theoretical energy required for the production of hydrogen (assuming 100% coulombic efficiency) when the channel depth is shrunk from 1.5 mm to 0.5 mm, 46.52 MJ·kg$_{H2}{}^{-1}$ and 45.37 MJ·kg$_{H2}{}^{-1}$, respectively. The theoretical energy required for hydrogen production for a current density value of 40 mA·cm^{-2} shows a larger difference of 4.2% when decreasing the channel depth from 1.5 mm to 0.5 mm, 39.93 MJ·kg$_{H2}{}^{-1}$ and 38.32 MJ·kg$_{H2}{}^{-1}$, respectively. For the sake of comparison, in the case of 1.0 mm channels the energy consumption is 45.47 MJ·kg$_{H2}{}^{-1}$ at 80 mA·cm^{-2} and 38.77 MJ·kg$_{H2}{}^{-1}$ at 40 mA·cm^{-2}.

However, above a current density of 80 mA·cm^{-2}, the voltage of the 1.0 mm polarization curve is lower than the values corresponding to the 0.5 mm and 1.5 mm curves. The difference between the results for 0.5 mm and 1.0 mm curves might be caused by the generation of CO_2, which is initially low but increases with current density [75,76]. From 80 mA·cm^{-2} onwards, more CO_2 is produced, and more bubbles appear, which makes mass transfer difficult when the channels are shallow. In this case, a decrease in anode channel depth can worsen performance. This is because, for a fixed value of current density, the CO_2 mass produced is the same, and when the channel depth is decreased, methanol may be clogged by these CO_2 bubbles more easily [39]. This generates longer gas slugs, hindering the methanol mass transfer from the channel to the catalytic layer. Increasing the channel depth from 1.0 mm to 1.5 mm results in an increase in cell voltage. This can be due to a lower fluid velocity in the 1.5 mm channels compared to the shallower channels [73]. The theoretical velocities and Reynolds numbers for channels with 0.5 mm, 1.0 mm and 1.5 mm depth are 0.10 m·s^{-1}, 0.05 m·s^{-1} and 0.03 m·s^{-1}, and 142.8, 107.1 and 85.7, respectively. As the liquid velocity decreases for deeper channels, the mass transfer between the channels and the gas diffusion layer (GDL) may worsen, as well as the transport under the ribs due to the decrease in pressure drop. These effects lead to an increase in the size of the CO_2 bubbles that prevent methanol from reaching the GDL. In this sense, Yang and Zhao [43] obtained satisfactory results in DMFC experiments with current densities up to 200 mA·cm^{-2} with Reynolds numbers around 30. Besides, the calculated Péclet number (Pe) remained constant across all configurations, suggesting similar advective-to-diffusive transport conditions. This supports the interpretation that the observed differences are primarily driven by geometric effects, particularly CO_2 bubble removal, rather than by changes in convective transport alone.

The effects observed in the polarization curves can also be analyzed with the comparison plots of minimum slope in the ohmic region and maximum power density at 300 mA·cm^{-2} presented in Figure 5. The slope for 1.0 mm depth has a shorter confidence interval and a lower value of the average minimum slope (closer to zero), which implies lower ohmic losses for this channel depth and a higher stability of the data between curves, with CO_2 bubbles having a smaller effect. When the power densities in Figure 5b are compared, the averages for 0.5 mm and 1.5 mm channel depth are higher than the average for 1.0 mm. This implies a higher energy consumption for very low or very high channel depths to produce the same theoretical amount of hydrogen.

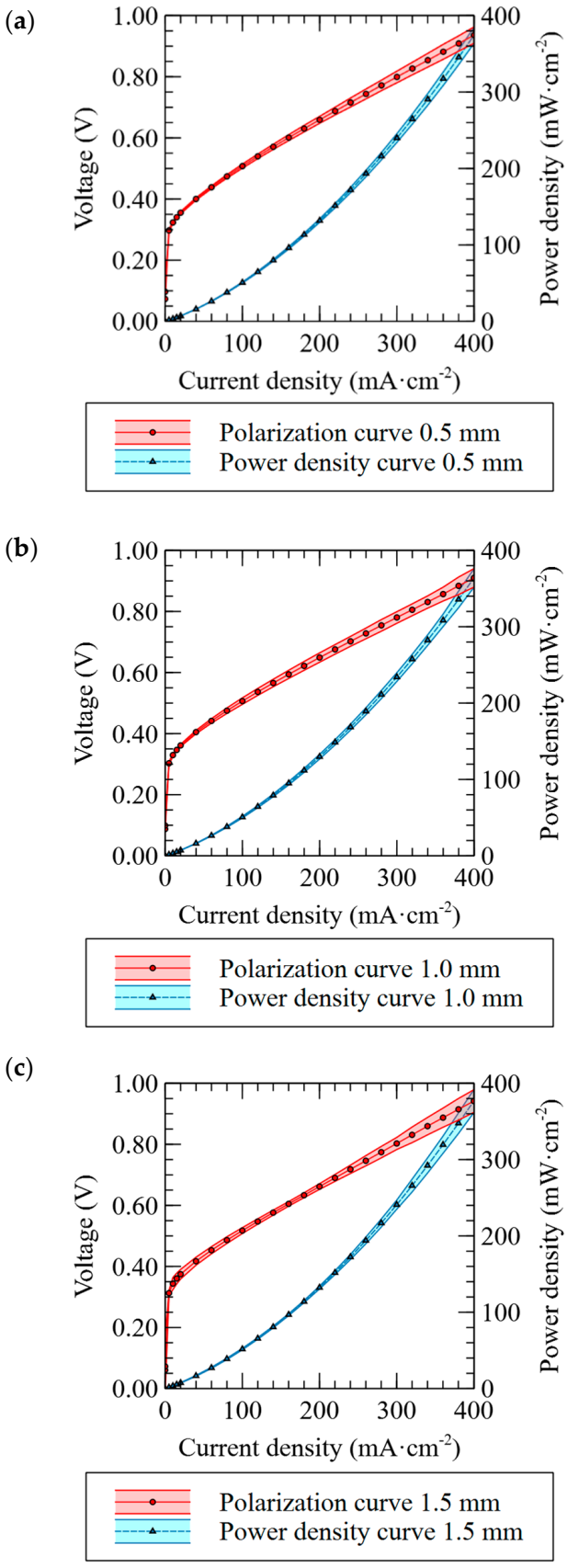

Figure 4. Polarization and power density curves of the MEC single-cell with anode channel depths of (**a**) 0.5 mm, (**b**) 1.0 mm and (**c**) 1.5 mm. Results obtained at a temperature of 60 °C, a methanol concentration of 1 M and methanol flow rate of 3 mL·min^{-1}.

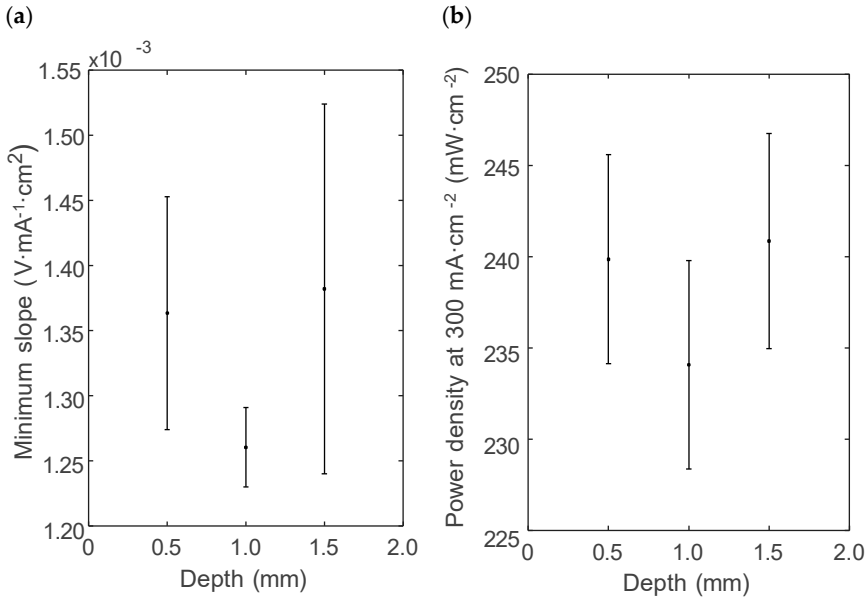

Figure 5. (**a**) Minimum slope of the MEC single-cell polarization curve in the ohmic region. (**b**) Maximum power density obtained from the MEC power density curve for a current density of 300 mA·cm^{-2}. Results obtained for anode channel depths of 0.5 mm, 1.0 mm and 1.5 mm at a temperature of 60 °C, a methanol concentration of 1 M and a methanol flow rate of 3 mL·min^{-1}.

The results presented for MECs with the three channel depths studied indicate that, working at low current densities, a MEC with a shallower anode channel depth performs better. However, when working at current densities higher than 80 mA·cm^{-2}, an intermediate anode channel depth of 1.0 mm shows better results, reducing the electrical energy needed to produce hydrogen from aqueous methanol.

3.3. Direct Methanol Fuel Cell

As can be seen in Figure 6, the shallowest anode channel depth studied, 0.5 mm, among those studied in this work, improves the performance of the DMFC single-cell, presenting a higher peak power density and greater data stability despite the higher influence and value of crossover at low current densities for shallower channels. This performance improvement could be attributed to the increase of flow velocity, the consequently pressure drop and the increase of mass transfer from the channels to the GDL. Additionally, a shallower channel results in a higher pressure drop between the two sides of the same rib favoring the transport of methanol under the rib, which is associated with a better removal of bubbles under this rib. The effect of channel depth on performance can be qualitatively explained for this case using two-phase flow theory. At a constant flow rate, decreasing channel depth reduces the cross-sectional area, increasing superficial velocity and promoting CO_2 bubble removal. This improves reactant access to the catalyst layer and reduces mass transfer resistance [39], as bubble blockage can be reduced.

For the 1.0 mm and 1.5 mm channel depths, the confidence intervals for both the polarization and power density curves are very wide. This reflects the instability of results obtained for various curves as CO_2 bubbles accumulate forming gas slugs due to lower fluid velocity, and methanol does not reach the GDL properly [77]. As the channel depth increases, the flow velocity decreases, reducing the flow of liquid present for the CO_2 bubbles to sweep up. During the polarization curve tests with a channel depth of 1.5 mm, CO_2 slug flow can be observed at the exit of the anode channel. This phenomenon could impede CO_2 removal, ultimately affecting DMFC performance and leading to a decrease in peak power density.

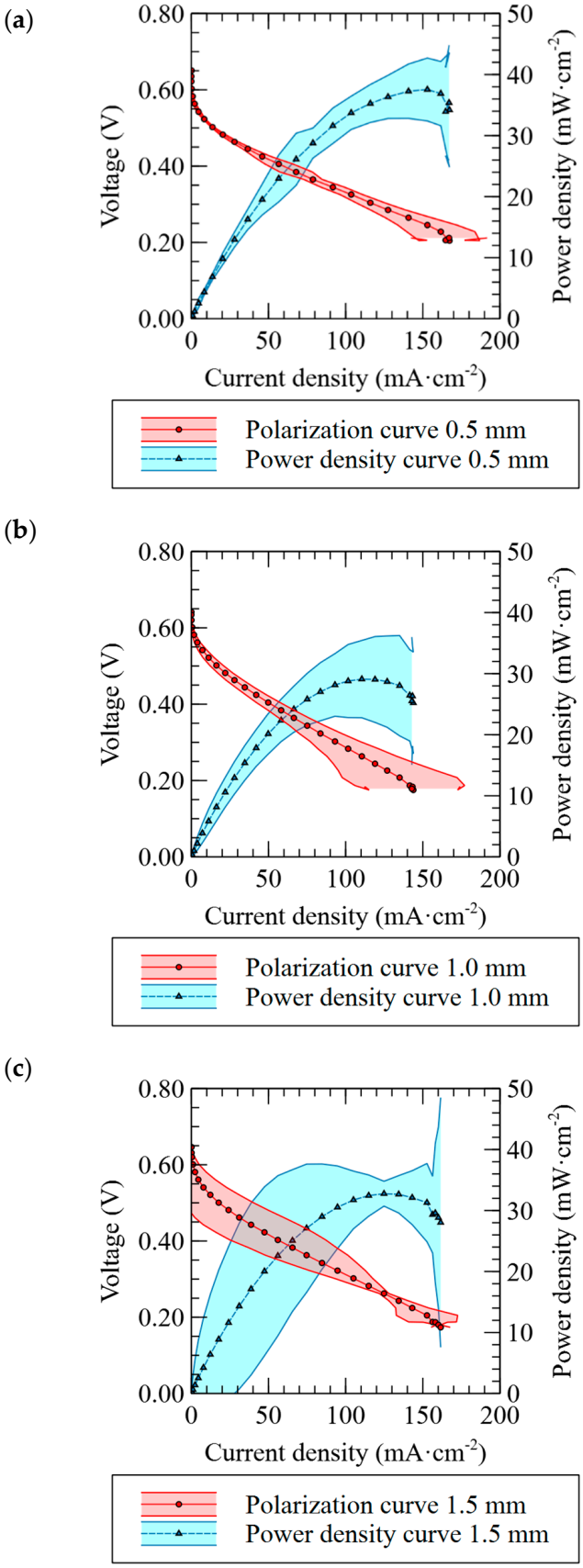

Figure 6. Polarization and power density curves of the DMFC single-cell with anode channel depths of (**a**) 0.5 mm, (**b**) 1.0 mm and (**c**) 1.5 mm. Results obtained at a temperature of 60 °C, cathode pressure 1 bar, oxygen flow rate of 110 mL·min^{-1}, a methanol concentration of 1 M and methanol flow rate of 3 mL·min^{-1}.

Furthermore, Figure 6 shows the increasing in the confidence interval amplitude as the current density increases. This phenomenon may be explained with the pressure drop variation due to increased bubble and gas slug generation. At lower current densities Wei Yuan et al. [77] reported a smaller variation of the pressure drop and bubble generation, being more important from a current density of 80 mA·cm^{-2} onwards.

Figure 7 shows the data derived from the analysis of the DMFC polarization curves obtained for each of the anode channel depths studied. As can be seen in Figure 7a, a shallower channel depth implies a smaller confidence interval in the maximum slope value, as well as a higher value of this parameter (closer to cero). As the anode channel depth increases, this slope decreases, implying more overpotential in the ohmic region. The ohmic region was selected to evaluate the maximum slope as it exhibits a linear voltage–current relationship primarily governed by internal resistances, such as membrane conductivity, contact resistance and electronic losses, whereas activation kinetics and mass transport limitations dominate the low and high-current regions, respectively. In Figure 7a results show that a shallower channel helps to reduce the ohmic polarization, improving the performance of the DMFC.

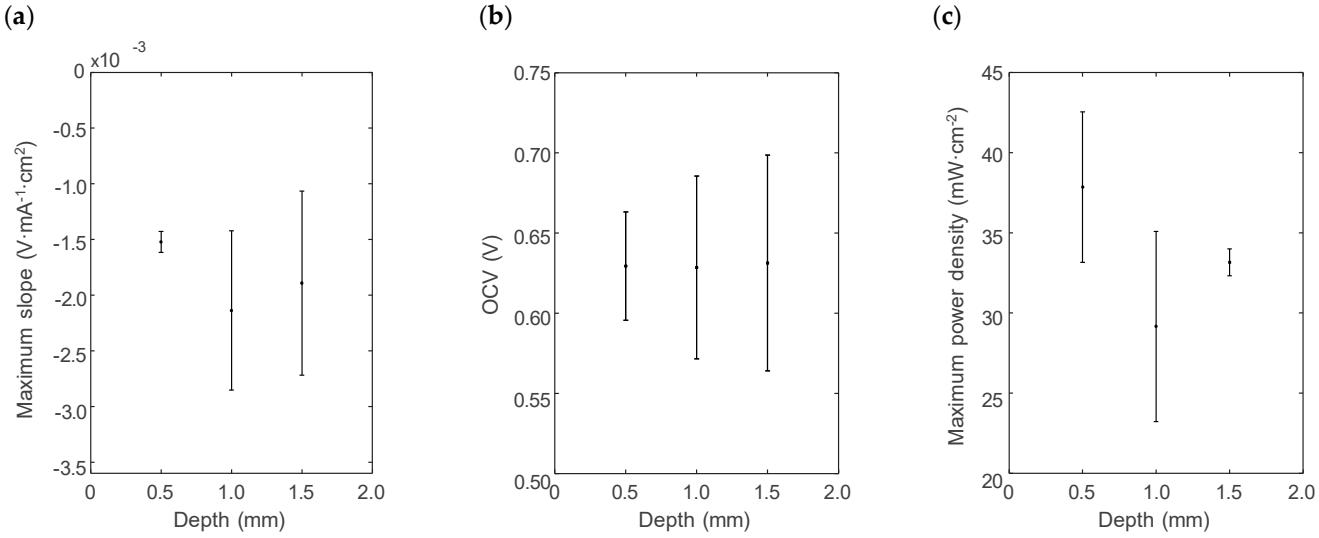

Figure 7. (**a**) Maximum slope of the DMFC single-cell polarization curve in the ohmic region. (**b**) Open circuit voltage of the DMFC single-cell polarization curve. (**c**) Peak power density obtained from the DMFC power density curve. Results obtained for anode channel depths of 0.5 mm, 1.0 mm and 1.5 mm, at a temperature of 60 °C, cathode pressure 0.1 MPa, oxygen flow rate of 110 mL·min^{-1}, methanol concentration of 1 M and methanol flow rate of 3 mL·min^{-1}.

In Figure 7b, a smaller variation in the open circuit voltage (OCV) data can be observed for a shallower channel depth. As the average OCV values are very close for the three channel depths, a larger confidence interval can imply either a lower OCV or a higher OCV for deeper channels. It is expected that increasing the channel depth will decrease the transport of fuel species from the anode to the cathode, which would imply a higher OCV.

The comparison in Figure 7c of the maximum power density obtained for each channel depth shows that the average for a shallower channel is higher, while the confidence interval of this parameter for the rest of the channel depths overlaps. This parameter is important in the choice of channel configuration to be used in a DMFC, and the results presented in this figure imply a higher power generation for shallower channels among those compared. However, despite the increase in average peak power density observed when moving from an anode channel depth of 1.5 mm to a depth of 0.5 mm, 33.2 mW·cm^{-2} and 37.9 mW·cm^{-2}, respectively, it should be noted that the decrease in channel depth also implies an increase in pressure drop along the channel. This, in turn, increases the

power required for pumping the methanol solution. Consequently, the overall efficiency of a DMFC system could decline with shallower channels. Furthermore, a lower channel depth than the 0.5 mm tested could produce a worse performance due to factors including methanol crossover and the void fraction of CO_2. For these reasons, future research should examine the trade-off between the advantages and disadvantages arising from the alteration in channel depth for a DMFC stack and its auxiliary systems.

Upon reviewing the outcomes outlined for MEC and DMFC, a distinct pattern emerges: an anode channel depth set at 0.5 mm proves most effective for DMFC single-cell, while MEC demonstrates superior performance with anode channel depth set at 1.0 mm. This may be due to the fact that for lower current densities (case of a DMFC) and therefore lower CO_2 production, a decrease in channel depth increases the velocity by keeping the volume flow rate constant, allowing the methanol to reach the GDL and quickly remove CO_2. However, increasing the current density (case of a MEC) increases the amount of CO_2 produced, and by decreasing the channel to 0.5 mm this CO_2 cannot be removed easily. In this case a change in the two-phase flow occurs, partially preventing the methanol oxidation reaction. This current density change can be observed in Figures 4 and 6, as under identical operating conditions (60 °C, 1M methanol and flow rate of 3 $mL \cdot min^{-1}$), the DMFC single-cell reached current densities in the range of 140 to 180 $mA \cdot cm^{-2}$, while the MEC achieved up to 400 $mA \cdot cm^{-2}$. These values reflect the fundamental difference between both systems: the MEC is externally powered and drives a non-spontaneous methanol electrolysis reaction, while the DMFC relies on the spontaneous oxidation of methanol coupled with oxygen reduction, as stated in Section 1.

4. Conclusions

This study systematically evaluated the impact of several anode channel depths on the performance of DMFC single-cells and, for the first time, of MEC single-cells, through the analysis of methanol crossover, polarization and power density curves. It was observed that shallower channels for DMFC increase methanol crossover but improve mass transfer efficiency, enhancing performance. However, shallower channels in the MEC worsen performance since a decrease in the depth at high current densities can produce that the channel may be clogged by CO_2 bubbles more easily. Deeper channels reduce crossover but face challenges in maintaining effective mass transfer, leading to performance deterioration in both cell types. Quantitatively, reducing the anode channel depth from 1.5 mm to 0.5 mm enhanced mass transfer efficiency, increasing the DMFC peak power density by 14.2% (from 33.2 to 37.9 $mW \cdot cm^{-2}$), while methanol crossover rose by 30.3%. In the MEC, this reduction in channel depth decreased the theoretical energy consumption for hydrogen production. These findings highlight the significant role of channel geometry in balancing mass transfer and crossover.

Channel depth of 0.5 mm exhibited superior performance in the DMFC, showcasing higher peak power density and improved stability despite increased crossover. The MEC with 0.5 mm anode channel depth demonstrated favorable voltage at lower current densities due to minimal CO_2 generation and increased methanol crossover. This crossover may result in an improvement in the electrochemical efficiency of hydrogen production, presenting a reduction of 4.2% in the theoretical energy required for the production of hydrogen when the channel depth is shrunk from 1.5 mm to 0.5 mm when working at 40 $mA \cdot cm^{-2}$. However, when the current density was increased, the 1.0 mm channel showcased sufficient velocity to enhance mass transfer from the channel to the GDL, making it the best option among those studied for MEC anode channels.

Shallower channel depths demonstrated enhanced mass transfer efficiency but increased methanol crossover, while deeper channels reduced crossover but suffered from

compromised mass transfer. These findings underscore the critical role of channel depth in efficiency of both DMFC and MEC single-cells. In this study different anode channel depths optimized performance for distinct electrochemical devices: 0.5 mm depth enhanced DMFC performance, whereas MEC exhibited superior performance with a 1.0 mm anode channel depth.

The influence of bubble regimes at different current densities on the behavior of DMFC and MEC, and their relationship with channel depth, flow velocity and pressure drop indicate the importance of studying these parameters for both devices. The effect of volumetric flow variation on the performance of both devices at different channel depths needs to be further studied, as well as its implication on the power consumption of systems based on these technologies. By studying this relationship, a solution could be found to increase the efficiency of systems based on the use of MECs and DMFCs. Besides, the implementation of electrochemical impedance spectroscopy (EIS) in future studies would help to decouple resistive losses and provide further insight into the role of channel geometry on cell performance.

From an application perspective, the findings of this work offer practical design guidelines for improving plate flow fields in compact methanol-based devices within the use of methanol as hydrogen carrier and energy vector. These insights support the development of portable DMFCs for low-power technologies, and MECs for decentralized hydrogen production in marine or mobile systems, where methanol logistics offer an advantage.

Author Contributions: V.L.M.: Conceptualization, Data curation, Formal analysis, Investigation, Methodology, Software, Validation, Visualization, Writing—original draft, Writing—Review & Editing. E.P.: Conceptualization, Investigation, Methodology, Writing—original draft, Writing—Review & Editing. A.V.-H.: Validation, Writing—Review & Editing. R.d.-D.: Validation, Writing—Review & Editing. T.J.L.: Writing—Review & Editing, Supervision, Validation, Project administration, Resources, Funding acquisition. Ó.S.: Conceptualization, Formal analysis, Methodology, Software, Validation, Supervision, Writing—original draft, Writing—Review & Editing. All authors have read and agreed to the published version of the manuscript.

Funding: This work has been carried out thanks to the Project GreenH2CM funded by MCIN/AEI/10.13039/501100011033, by "NextGenerationEU/PRTR" and the Regional Government of Madrid and to the Grant PID2021-124263OB-I00 funded by MCIN/AEI/10.13039/501100011033 and by "ERDF a way of making Europe".

Data Availability Statement: The raw data supporting the conclusions of this article will be made available by the authors on request.

Conflicts of Interest: The authors declare no conflicts of interest.

Abbreviations

The following abbreviations are used in this manuscript:

DMFC	Direct Methanol Fuel Cell
GDL	Gas Diffusion Layer
MEC	Methanol Electrolysis Cell
MEA	Membrane Electrode Assembly
OCV	Open Circuit Voltage
SS316L	Stainless Steel 316L

References

1. Kamarudin, S.K.; Achmad, F.; Daud, W.R.W. Overview on the application of direct methanol fuel cell (DMFC) for portable electronic devices. *Int. J. Hydrogen Energy* **2009**, *34*, 6902–6916. [CrossRef]
2. Sun, C.; Negro, E.; Vezzù, K.; Pagot, G.; Cavinato, G.; Nale, A.; Bang, Y.H.; Di Noto, V. Hybrid inorganic-organic proton-conducting membranes based on SPEEK doped with WO3 nanoparticles for application in vanadium redox flow batteries. *Electrochim. Acta* **2019**, *309*, 311–325. [CrossRef]
3. Chen, C.; Lu, Y.; Xing, L. Levelling renewable power output using hydrogen-based storage systems: A techno-economic analysis. *J. Energy Storage* **2021**, *37*, 102413. [CrossRef]
4. Sarlak, G.; Olamaei, J.; Dosaranian-Moghadam, M. Optimal Management of Multi-Carrier Energy Hub Regarding Fuel Cell and, Storage Technologies. *J. Energy Storage* **2022**, *46*, 103821. [CrossRef]
5. Marzouk, O.A. Power Density and Thermochemical Properties of Hydrogen Magnetohydrodynamic (H2MHD) Generators at Different Pressures, Seed Types, Seed Levels, and Oxidizers. *Hydrogen* **2025**, *6*, 31. [CrossRef]
6. Fang, S.; Song, N.; Liu, Y.; Zhao, C.; Wang, Y. Comprehensive energy conversion efficiency analysis of micro direct methanol fuel cell stack based on polarization theory. *Energy* **2024**, *287*, 129670. [CrossRef]
7. Chen, P.S.-L.; Fan, H.; Enshaei, H.; Zhang, W.; Shi, W.; Abdussamie, N.; Miwa, T.; Qu, Z.; Yang, Z. Opportunities and Challenges of Hydrogen Ports: An Empirical Study in Australia and Japan. *Hydrogen* **2024**, *5*, 436–458. [CrossRef]
8. Mucci, S.; Mitsos, A.; Bongartz, D. Cost-optimal Power-to-Methanol: Flexible operation or intermediate storage? *J. Energy Storage* **2023**, *72*, 108614. [CrossRef]
9. Fadzillah, D.; Kamarudin, S.; Zainoodin, M.; Masdar, M. Critical challenges in the system development of direct alcohol fuel cells as portable power supplies: An overview. *Int. J. Hydrogen Energy* **2019**, *44*, 3031–3054. [CrossRef]
10. Araya, S.S.; Liso, V.; Cui, X.; Li, N.; Zhu, J.; Sahlin, S.L.; Jensen, S.H.; Nielsen, M.P.; Kær, S.K. A Review of The Methanol Economy: The Fuel Cell Route. *Energies* **2020**, *13*, 596. [CrossRef]
11. Edwards, P.P.; Kuznetsov, V.L.; David, W.I.F.; Brandon, N.P. Hydrogen and fuel cells: Towards a sustainable energy future. *Energy Policy* **2008**, *36*, 4356–4362. [CrossRef]
12. Roode-Gutzmer, Q.I.; Kaiser, D.; Bertau, M. Renewable Methanol Synthesis. *ChemBioEng Rev.* **2019**, *6*, 209–236. [CrossRef]
13. Moellenbruck, F.; Kempken, T.; Dierks, M.; Oeljeklaus, G.; Goerner, K. Cogeneration of power and methanol based on a conventional power plant in Germany. *J. Energy Storage* **2018**, *19*, 393–401. [CrossRef]
14. Shi, L.; Wang, C.; Liu, S.; Cheng, X.; Liu, Q.; Zhuge, W.; Zhang, Y. Energy optimization and economic study of an energy storage system based on a carbon dioxide-to-methanol process. *J. Energy Storage* **2023**, *62*, 106846. [CrossRef]
15. Zhang, Y.; Wang, H.; Li, R.; Wang, Z.; Ling, L.; Jin, P.; Wang, H. An electro-hydrogen cogeneration system combining compressed air energy storage and methanol cracking reaction. *J. Energy Storage* **2023**, *58*, 106351. [CrossRef]
16. Liu, Q.; Du, S.; Liu, T.; Gong, L.; Wu, Y.; Lin, J.; Yang, P.; Huang, G.; Li, M.; Wu, Y.; et al. Efficient Low-temperature Hydrogen Production by Electrochemical-assisted Methanol Steam Reforming. *Angew. Chem. Int. Ed. Engl.* **2024**, *63*, e202315157. [CrossRef] [PubMed]
17. Ruiz-López, E.; Caravaca, A.; Vernoux, P.; Dorado, F.; de Lucas-Consuegra, A. Over-faradaic hydrogen production in methanol electrolysis cells. *Chem. Eng. J.* **2020**, *396*, 125217. [CrossRef]
18. Kuramochi, N.; Yoshida-Hirahara, M.; Ogihara, H.; Kurokawa, H. Proton exchange membrane electrolysis of methanol for simultaneously synthesizing formaldehyde and hydrogen. *Sustain. Energy Fuels* **2023**, *7*, 778–785. [CrossRef]
19. Gong, A.; Verstraete, D. Fuel cell propulsion in small fixed-wing unmanned aerial vehicles: Current status and research needs. *Int. J. Hydrogen Energy* **2017**, *42*, 21311–21333. [CrossRef]
20. Eqbal, M.A.S.; Fernando, N.; Marino, M.; Wild, G. Hybrid Propulsion Systems for Remotely Piloted Aircraft Systems. *Aerospace* **2018**, *5*, 34. [CrossRef]
21. Kim, T.; Kwon, S. Design and development of a fuel cell-powered small unmanned aircraft. *Int. J. Hydrogen Energy* **2012**, *37*, 615–622. [CrossRef]
22. Yagiz, M.; Çelik, S.; Topcu, A. Performance comparison of bio-inspired flow field designs for direct methanol fuel cell and proton exchange membrane fuel cell. *Int. J. Hydrogen Energy* **2024**, *75*, 200–210. [CrossRef]
23. Sesu, D.C.; Narendran, G.; Ramakrishnan, S.; Vediappan, K.; Muthu, S.E.; Shanmugan, S.; Kannan, K. Design and Fabrication of Micro-Electromechanical System (MEMS)-Based μ-DMFC (Direct Methanol Fuel Cells) for Portable Applications: An Outlook. *Electrochem* **2025**, *6*, 11. [CrossRef]
24. Ahmed, M.; Dincer, I. A review on methanol crossover in direct methanol fuel cells: Challenges and achievements. *Int. J. Energy Res.* **2011**, *35*, 1213–1228. [CrossRef]
25. Goor, M.; Menkin, S.; Peled, E. High power direct methanol fuel cell for mobility and portable applications. *Int. J. Hydrogen Energy* **2019**, *44*, 3138–3143. [CrossRef]
26. Alias, M.; Kamarudin, S.; Zainoodin, A.; Masdar, M. Active direct methanol fuel cell: An overview. *Int. J. Hydrogen Energy* **2020**, *45*, 19620–19641. [CrossRef]

27. Barbera, O.; Stassi, A.; Sebastian, D.; Bonde, J.; Giacoppo, G.; D'Urso, C.; Baglio, V.; Arico', A.S. Simple and functional direct methanol fuel cell stack designs for application in portable and auxiliary power units. *Int. J. Hydrogen Energy* **2016**, *41*, 12320–12329. [CrossRef]
28. Baglio, V.; Stassi, A.; Matera, F.; Antonucci, V.; Aricò, A. Investigation of passive DMFC mini-stacks at ambient temperature. *Electrochim. Acta* **2009**, *54*, 2004–2009. [CrossRef]
29. Wang, L.; He, M.; Hu, Y.; Zhang, Y.; Liu, X.; Wang, G. A "4-cell" modular passive DMFC (direct methanol fuel cell) stack for portable applications. *Energy* **2015**, *82*, 229–235. [CrossRef]
30. Kim, D.; Lee, J.; Lim, T.-H.; Oh, I.-H.; Ha, H.Y. Operational characteristics of a 50 W DMFC stack. *J. Power Sources* **2006**, *155*, 203–212. [CrossRef]
31. Joh, H.-I.; Hwang, S.Y.; Cho, J.H.; Ha, T.J.; Kim, S.-K.; Moon, S.H.; Ha, H.Y. Development and characteristics of a 400 W-class direct methanol fuel cell stack. *Int. J. Hydrogen Energy* **2008**, *33*, 7153–7162. [CrossRef]
32. Berretti, E.; Osmieri, L.; Baglio, V.; Miller, H.A.; Filippi, J.; Vizza, F.; Santamaria, M.; Specchia, S.; Santoro, C.; Lavacchi, A. Direct Alcohol Fuel Cells: A Comparative Review of Acidic and Alkaline Systems. *Electrochem. Energy Rev.* **2023**, *6*, 30. [CrossRef]
33. Villalba-Herreros, A.; Santiago, Ó.; Abad, R.; Leo, T.J. Carbon dioxide treatment method for autonomous underwater vehicles powered by direct methanol fuel cells: A multi-criteria decision analysis approach. *J. Power Sources* **2021**, *512*, 230322. [CrossRef]
34. Ozden, A.; Ercelik, M.; Ouellette, D.; Colpan, C.O.; Ganjehsarabi, H.; Hamdullahpur, F. Designing, modeling and performance investigation of bio-inspired flow field based DMFCs. *Int. J. Hydrogen Energy* **2017**, *42*, 21546–21558. [CrossRef]
35. Oliveira, V.; Rangel, C.; Pinto, A. Effect of anode and cathode flow field design on the performance of a direct methanol fuel cell. *Chem. Eng. J.* **2010**, *157*, 174–180. [CrossRef]
36. Chen, M.; Wang, M.; Yang, Z.; Ding, X.; Wang, X. Long-term degradation behaviors research on a direct methanol fuel cell with more than 3000 h lifetime. *Electrochim. Acta* **2018**, *282*, 702–710. [CrossRef]
37. Ouellette, D.; Ozden, A.; Ercelik, M.; Colpan, C.O.; Ganjehsarabi, H.; Li, X.; Hamdullahpur, F. Assessment of different bio-inspired flow fields for direct methanol fuel cells through 3D modeling and experimental studies. *Int. J. Hydrogen Energy* **2018**, *43*, 1152–1170. [CrossRef]
38. Aricò, A.; Cretì, P.; Baglio, V.; Modica, E.; Antonucci, V. Influence of flow field design on the performance of a direct methanol fuel cell. *J. Power Sources* **2000**, *91*, 202–209. [CrossRef]
39. Vijayakumar, R.; Rajkumar, M.; Sridhar, P.; Pitchumani, S. Effect of anode and cathode flow field depths on the performance of liquid feed direct methanol fuel cells (DMFCs). *J. Appl. Electrochem.* **2012**, *42*, 319–324. [CrossRef]
40. Jung, D.Y.; Song, D.K.; Kim, J.S.; Lee, S.H.; Min, G.W.; Son, J.H.; Cho, G.Y. Numerical Investigation of Effects of Obstacles in Flow Channels and Depth of Flow Channels for PEMFCs. *Sustainability* **2024**, *16*, 10144. [CrossRef]
41. Pham, A.T.; Baba, T.; Shudo, T. Efficient hydrogen production from aqueous methanol in a PEM electrolyzer with porous metal flow field: Influence of change in grain diameter and material of porous metal flow field. *Int. J. Hydrogen Energy* **2013**, *38*, 9945–9953. [CrossRef]
42. Yuan, Z.; Zhang, Y.; Fu, W.; Li, Z.; Liu, X. Investigation of a small-volume direct methanol fuel cell stack for portable applications. *Energy* **2013**, *51*, 462–467. [CrossRef]
43. Yang, H.; Zhao, T. Effect of anode flow field design on the performance of liquid feed direct methanol fuel cells. *Electrochim. Acta* **2005**, *50*, 3243–3252. [CrossRef]
44. Ramasamy, J.; Palaniswamy, K.; Kumaresan, T.; Chandran, M.; Chen, R. Study of novel flow channels influence on the performance of direct methanol fuel cell. *Int. J. Hydrogen Energy* **2022**, *47*, 595–609. [CrossRef]
45. Chowdhury, P.R.; Gladen, A.C. Empirical Comparison of Flow Field Designs for Direct Ethanol-Based, High-Temperature PEM Fuel Cells. *Fuels* **2025**, *6*, 46. [CrossRef]
46. Vuppala, R.K.S.S.; Chaedir, B.A.; Jiang, L.; Chen, L.; Aziz, M.; Sasmito, A.P. Optimization of Membrane Electrode Assembly of PEM Fuel Cell by Response Surface Method. *Molecules* **2019**, *24*, 3097. [CrossRef] [PubMed]
47. Song, Y.; Zhang, C.; Ling, C.-Y.; Han, M.; Yong, R.-Y.; Sun, D.; Chen, J. Review on current research of materials, fabrication and application for bipolar plate in proton exchange membrane fuel cell. *Int. J. Hydrogen Energy* **2020**, *45*, 29832–29847. [CrossRef]
48. Scott, K.; Argyropoulos, P.; Yiannopoulos, P.; Taama, W. Electrochemical and gas evolution characteristics of direct methanol fuel cells with stainless steel mesh flow beds. *J. Appl. Electrochem.* **2001**, *31*, 823–832. [CrossRef]
49. Tawfik, H.; Hung, Y.; Mahajan, D. Metal bipolar plates for PEM fuel cell—A review. *J. Power Sources* **2007**, *163*, 755–767. [CrossRef]
50. Yu, B.; Yang, Q.; Kianimanesh, A.; Freiheit, T.; Park, S.; Zhao, H.; Xue, D. A CFD model with semi-empirical electrochemical relationships to study the influence of geometric and operating parameters on DMFC performance. *Int. J. Hydrogen Energy* **2013**, *38*, 9873–9885. [CrossRef]
51. Calabriso, A.; Borello, D.; Cedola, L.; Del Zotto, L.; Santori, S.G. Assessment of CO_2 Bubble Generation Influence on Direct Methanol Fuel Cell Performance. *Energy Procedia* **2015**, *75*, 1996–2002. [CrossRef]
52. Calabriso, A.; Borello, D.; Romano, G.P.; Cedola, L.; Del Zotto, L.; Santori, S.G. Bubbly flow mapping in the anode channel of a direct methanol fuel cell via PIV investigation. *Appl. Energy* **2017**, *185*, 1245–1255. [CrossRef]

53. Park, Y.-C.; Chippar, P.; Kim, S.-K.; Lim, S.; Jung, D.-H.; Ju, H.; Peck, D.-H. Effects of serpentine flow-field designs with different channel and rib widths on the performance of a direct methanol fuel cell. *J. Power Sources* **2012**, *205*, 32–47. [CrossRef]
54. Carey, V.P. Liquid-Vapor Phase-Change Phenomena: An Introduction to the Thermophysics of Vaporization and Condensation Processes in Heat Transfer Equipment. In *Liquid-Vapor Phase-Change Phenomena, 3rd ed*; CRC Press: Boca Raton, FL, USA, 2020. [CrossRef]
55. Uhm, S.; Jeon, H.; Kim, T.J.; Lee, J. Clean hydrogen production from methanol–water solutions via power-saved electrolytic reforming process. *J. Power Sources* **2012**, *198*, 218–222. [CrossRef]
56. Sasikumar, G.; Muthumeenal, A.; Pethaiah, S.; Nachiappan, N.; Balaji, R. Aqueous methanol eletrolysis using proton conducting membrane for hydrogen production. *Int. J. Hydrogen Energy* **2008**, *33*, 5905–5910. [CrossRef]
57. Take, T.; Tsurutani, K.; Umeda, M. Hydrogen production by methanol–water solution electrolysis. *J. Power Sources* **2007**, *164*, 9–16. [CrossRef]
58. Meca, V.L.; D'aMore-Domenech, R.; Crucelaegui, A.; Leo, T.J. Large-Scale Maritime Transport of Hydrogen: Economic Comparison of Liquid Hydrogen and Methanol. *ACS Sustain. Chem. Eng.* **2022**, *10*, 4300–4311. [CrossRef]
59. Li, L.; Zhang, L.; Gou, L.; Wei, S.; Hou, X.; Wu, L. High-performance methanol electrolysis towards energy-saving hydrogen production: Using Cu2O-Cu decorated Ni2P nanoarray as bifunctional monolithic catalyst. *Chem. Eng. J.* **2023**, *454*, 140292. [CrossRef]
60. Sanchez, C.; Espinos, F.J.; Barjola, A.; Escorihuela, J.; Compañ, V. Hydrogen Production from Methanol–Water Solution and Pure Water Electrolysis Using Nanocomposite Perfluorinated Sulfocationic Membranes Modified by Polyaniline. *Polymers* **2022**, *14*, 4500. [CrossRef] [PubMed]
61. Pham, A.T.; Baba, T.; Sugiyama, T.; Shudo, T. Efficient hydrogen production from aqueous methanol in a PEM electrolyzer with porous metal flow field: Influence of PTFE treatment of the anode gas diffusion layer. *Int. J. Hydrogen Energy* **2013**, *38*, 73–81. [CrossRef]
62. Lamy, C.; Coutanceau, C.; Baranton, S. Production of hydrogen by the electrocatalytic oxidation of low-weight compounds (HCOOH, MeOH, EtOH). In *Production of Clean Hydrogen by Electrochemical Reforming of Oxygenated Organic Compounds*; Elsevier: San Diego, CA, USA, 2020; pp. 37–79. [CrossRef]
63. Sethu, S.P.; Gangadharan, S.; Chan, S.H.; Stimming, U. Development of a novel cost effective methanol electrolyzer stack with Pt-catalyzed membrane. *J. Power Sources* **2014**, *254*, 161–167. [CrossRef]
64. Pethaiah, S.S.; Sadasivuni, K.K.; Jayakumar, A.; Ponnamma, D.; Tiwary, C.S.; Sasikumar, G. Methanol Electrolysis for Hydrogen Production Using Polymer Electrolyte Membrane: A Mini-Review. *Energies* **2020**, *13*, 5879. [CrossRef]
65. Hu, Z.; Wu, M.; Wei, Z.; Song, S.; Shen, P.K. Pt-WC/C as a cathode electrocatalyst for hydrogen production by methanol electrolysis. *J. Power Sources* **2007**, *166*, 458–461. [CrossRef]
66. Egea, J.R.J.; Martín, E.C.; Bas, M.T.C. Procedimiento de Obtención de Recubrimiento Mediante Técnica de Aerografiado Automático a Partir de Suspensiones de Polvos Nanométricos o Soles Obtenidos vía Sol-Gel y Dispositivo Para su Puesta a Punto, 2209657. 2004. Available online: https://worldwide.espacenet.com/publicationDetails/originalDocument?FT=D&date=20040616&DB=EPODOC&locale=&CC=ES&NR=2209657A1&KC=A1&ND=2 (accessed on 20 December 2023).
67. Leo, T.; Raso, M.; Navarro, E.; de la Blanca, E.S.; Villanueva, M.; Moreno, B. Response of a direct methanol fuel cell to fuel change. *Int. J. Hydrogen Energy* **2010**, *35*, 11642–11648. [CrossRef]
68. Meca, V.L.; D'Amore-Domenech, R.; Villalba-Herreros, A.; Leo, T.J. Test bench for electricity or hydrogen production from aqueous methanol. In Proceedings of the 36th International Conference on Efficiency, Cost, Optimization, Simulation and Environmental Impact of Energy Systems, Las Palmas de Gran Canaria, Spain, 25–30 June 2023; pp. 1104–1109. [CrossRef]
69. Ren, X.; Springer, T.E.; Zawodzinski, T.A.; Gottesfeld, S. Methanol Transport Through Nation Membranes. Electro-osmotic Drag Effects on Potential Step Measurements. *J. Electrochem. Soc.* **2000**, *147*, 466. [CrossRef]
70. Santiago, Ó.; Mosa, J.; Escribano, P.; Navarro, E.; Chinarro, E.; Aparicio, M.; Leo, T.; del Río, C. $40SiO_2$–$40P_2O_5$–$20ZrO_2$ sol-gel infiltrated sSEBS membranes with improved methanol crossover and cell performance for direct methanol fuel cell applications. *Int. J. Hydrogen Energy* **2020**, *45*, 20620–20631. [CrossRef]
71. Basile, A.; Dalena, F. *Methanol: Science and Engineering*, 1st ed.; Elsevier: Amsterdam, The Netherlands, 2017.
72. Pinto, A.M.F.R.; Oliveira, V.B.; Falcão, D.S. *Direct Alcohol Fuel Cells for Portable Applications: Fundamentals, Engineering and Advances*; Academic Press: Cambridge, MA, USA, 2018. [CrossRef]
73. Park, J.-Y.; Seo, Y.; Kang, S.; You, D.; Cho, H.; Na, Y. Operational characteristics of the direct methanol fuel cell stack on fuel and energy efficiency with performance and stability. *Int. J. Hydrogen Energy* **2012**, *37*, 5946–5957. [CrossRef]
74. Lamy, C.; Guenot, B.; Cretin, M.; Pourcelly, G. (Invited) A Kinetics Analysis of Methanol Oxidation under Electrolysis/Fuel Cell Working Conditions. *ECS Trans.* **2015**, *66*, 1–12. [CrossRef]
75. Yang, H.; Zhao, T.; Ye, Q. In situ visualization study of CO_2 gas bubble behavior in DMFC anode flow fields. *J. Power Sources* **2005**, *139*, 79–90. [CrossRef]

76. Su, X.; Yuan, W.; Lu, B.; Zheng, T.; Ke, Y.; Zhuang, Z.; Zhao, Y.; Tang, Y.; Zhang, S. CO_2 bubble behaviors and two-phase flow characteristics in single-serpentine sinusoidal corrugated channels of direct methanol fuel cell. *J. Power Sources* **2020**, *450*, 227621. [CrossRef]
77. Yuan, W.; Wang, A.; Ye, G.; Pan, B.; Tang, K.; Chen, H. Dynamic relationship between the CO_2 gas bubble behavior and the pressure drop characteristics in the anode flow field of an active liquid-feed direct methanol fuel cell. *Appl. Energy* **2017**, *188*, 431–443. [CrossRef]